Journal of Materials Science: Materials in Electronics (2019) 30:14077–14084
https://doi.org/10.1007/s10854-019-01773-4

Microstructure and shear behavior of solder joint with Sn58Bi/Sn3.0Ag0.5Cu/Cu superposition structure

Yang Liu[1] · Ruisheng Xu[1] · Hao Zhang[1] · Fenglian Sun[1]

Received: 6 May 2019 / Accepted: 27 June 2019 / Published online: 1 July 2019

Abstract
Solder joint with Sn58Bi/Sn3.0Ag0.5Cu/Cu superposition structure was designed and fabricated by two-step soldering process. Sn, Ag, and Cu atoms diffused from the Sn3.0Ag0.5Cu bulk into the molten Sn58Bi solder paste during the second soldering process. The Sn3.0Ag0.5Cu bulk in the composite solder joint increased the concentration and grain size of β-Sn in the Sn58Bi bulk. Moreover, a large amount of tiny Bi-rich particles were found in the Sn58Bi solder bulk. The formation and growth of the β-Sn phases in the Sn58Bi solder bulk was affected by the microstructure of the Sn3.0Ag0.5Cu bulk. Additionally, the β-Sn dendritic in Sn58Bi bulk grew along the Sn3.0Ag0.5Cu bulk like the sunlight. The composite solder joint showed more ductile features than the traditional Sn58Bi eutectic solder joint due to its microstructural transformation occurred during the second soldering process. The Sn3.0Ag0.5Cu bulk with superposition structure works as a barrier to propagate cracks and effectively suppresses the brittle failure of the solder joint.

1 Introduction

In order to meet the tendency of miniaturization and densification of electronic products, the requirements for packaging technology and materials are becoming increasingly higher. The performance of solder joints has a great impact on the reliability of a whole packaging system. As one of the common lead-free solder materials, Sn58Bi (SnBi) has been widely investigated and used due to its low melting temperature and low cost. However, a critical disadvantage of SnBi solder joint is its brittleness induced from the inherent brittleness of Bi element. Liu and Shang [1] found that bismuth segregation occurs at the copper-intermetallic interface upon thermal aging. It exacerbates the interfacial brittleness and results in a sharp decrease in fatigue and fracture resistance of the solder joint. Therefore, it is of great significance to suppress the brittleness and improve the comprehensive performance of SnBi solder joint for its wide applications.

Many researches incorporated additional alloying elements or particles into SnBi solder material. Li and Chan [2] studied the effects of Ag nanoparticles addition on the microstructural and mechanical properties of SnBi composite solder joints. Their results indicated that the added Ag nanoparticles refined the matrix microstructure of SnBi solder, enhanced the microhardness, suppressed the interfacial intermetallic compound (IMC) growth and reinforced the shear strength of the solder joints. Ma and Wu [3] added 0.7 wt% Zn into the SnBi solder paste. The coarsening of Bi-rich phases and the growth of IMC in SnBi/Cu solder joints were suppressed. Besides, the ultimate tensile strength (UTSs) of the SnBi solder slab was also increased by 6.05% after soldering. In the study of Zhu et al. [4], Al_2O_3 nanoparticles with various contents (0, 0.5, 1.0, 1.5 wt%) were added into SnBi solder paste. The results showed that moderate amount of Al_2O_3 nanoparticles addition promoted the even distribution of Sn-rich and Bi-rich phases after soldering. Compared with the SnBi solder joint, the UTSs and hardness of SnBi–0.5Al_2O_3 solder joint were enhanced. Sun et al. [5] analyzed the mechanical properties of SnBi solder joint doped with various amounts of carbon nanotubes (CNTs). The highest shear strength of 77.3 MPa was obtained after adding 0.05 wt% CNTs. However, the shear strength of SnBi solder joint decreased sharply when the doping amount overpassed 0.1 wt%. Liu et al. [6] fabricated the SnBi composite solder paste by adding various amounts of Sn–Ag–Cu–Bi–Ni (SAC-BN) particles through mechanical mixing method. As the content of SAC-BN particles increased from 0 to 8 wt%, the concentration and size of

✉ Yang Liu
lyang805@163.com

[1] School of Materials Science and Engineering, Harbin University of Science and Technology, Harbin 150040, China

β-Sn increased in the solder bulks after soldering while the hardness and elastic modulus showed a decrease trend.

Another effective way to improve the properties of SnBi solder joint is to modify the surface finish or composition of substrate. The common surface finishes include organic solderability preservative (OSP), electroless nickel-immersion gold (ENIG), and electroless nickel-electroless palladium-immersion gold (ENEPIG) [7]. Besides, Wang et al. [8] obtained Sn–Ag–Cu surface finish with the thickness of 5 μm on Cu. This surface finish was found to be helpful to inhibit the growth of interfacial IMC layer during isothermal aging. Hu et al. [9] and Zou et al. [10] added trace amounts of Ag, Al, Sn or Zn elements into Cu substrate, and found the interfacial Bi embrittlement in SnBi/Cu was restrained. Meanwhile, the void at the interface was eliminated.

This study aimed to suppress the interfacial brittleness of SnBi solder joint by structure and soldering process design. Therefore, solder joint with SnBi/SnAgCu/Cu superposition structure was proposed. The microstructure and shear behavior of this type of solder joint was investigated in comparison with SnBi/Cu and SnAgCu/Cu.

2 Experimental procedure

The solder materials used in this work are commercial Sn3.0Ag0.5Cu (SAC) solder ball and Sn58Bi solder paste. The soldering substrates are Cu pads with the diameter of 460 μm on printed circuit board (PCB). Firstly, SAC balls with diameter of 300 μm were soldered onto the Cu pads by a heating platform at 260 °C for 80 s. The soldered samples were put into anhydrous ethanol and cleaned for 10 min by ultrasonic. Secondly, SnBi solder paste was dispensed onto the soldered SAC joints by Create-PSD solder paste dispenser. The samples were soldered at 160 °C for 80 s and formed the solder joints with superposition structure. The manufacturing process and schematic diagram of this structure are shown in Fig. 1. For comparison purpose, SAC/Cu and SnBi/Cu solder joints were soldered at 260 °C and 160 °C for 80 s respectively. Here the ball height of all the three kinds of solder joints is 470 μm.

Cross-sections of the solder joints were prepared following the grinding and polishing processes. Optical microscope, scanning electron microscopy (SEM), and energy dispersive X-ray spectroscope (EDS) were used for the materials characterization. The shear test was conducted by RESCH PTR-1000 tester according to JESD22-B117B-2014 standard. The shear height was set as 45 μm and the shear speed was 0.1 mm/s. The shear fractures were observed with SEM and KEYENCE super resolution digital microscope.

3 Results and discussion

3.1 Microstructure of the solder joints

Figure 2a–c presents the overall optical microstructure of the three kinds of solder joints. Compared with SnBi/Cu and SAC/Cu couples, the composite solder joint in Fig. 2c shows different morphology. SnBi/SAC/Cu superposition structure could be seen clearly through the cross-sectional observation. Figure 2d–f shows the SEM micrographs of the magnified areas noted in Fig. 2a–c respectively. As shown in Fig. 2d, β-Sn and Bi-rich phases form a typical reticulate structure of SnBi eutectic solder joints as reported by literatures [11, 12]. The solder bulk in the SAC/Cu joint is composed of β-Sn and eutectic phases as presented in Fig. 2e. This structure is also in agreement with the reported works [13, 14]. Compared with Fig. 2d, e, f shows different microstructure. Large β-Sn grains could be observed in this structure. Meanwhile, these β-Sn grains consist of some tiny Bi-rich phases.

Figure 3 shows a cross-sectional SEM image and element mapping of the composite solder joint. The Sn and

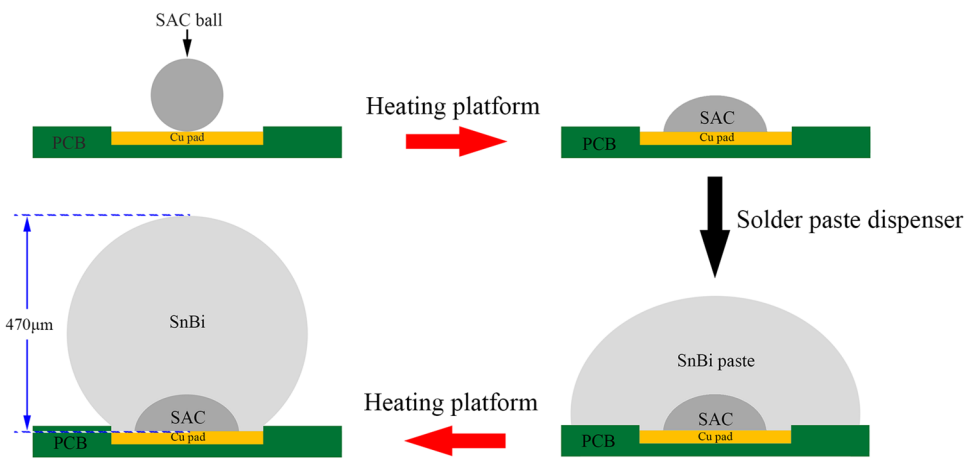

Fig. 1 Manufacturing process and schematic diagram of SnBi/SAC/Cu solder joint

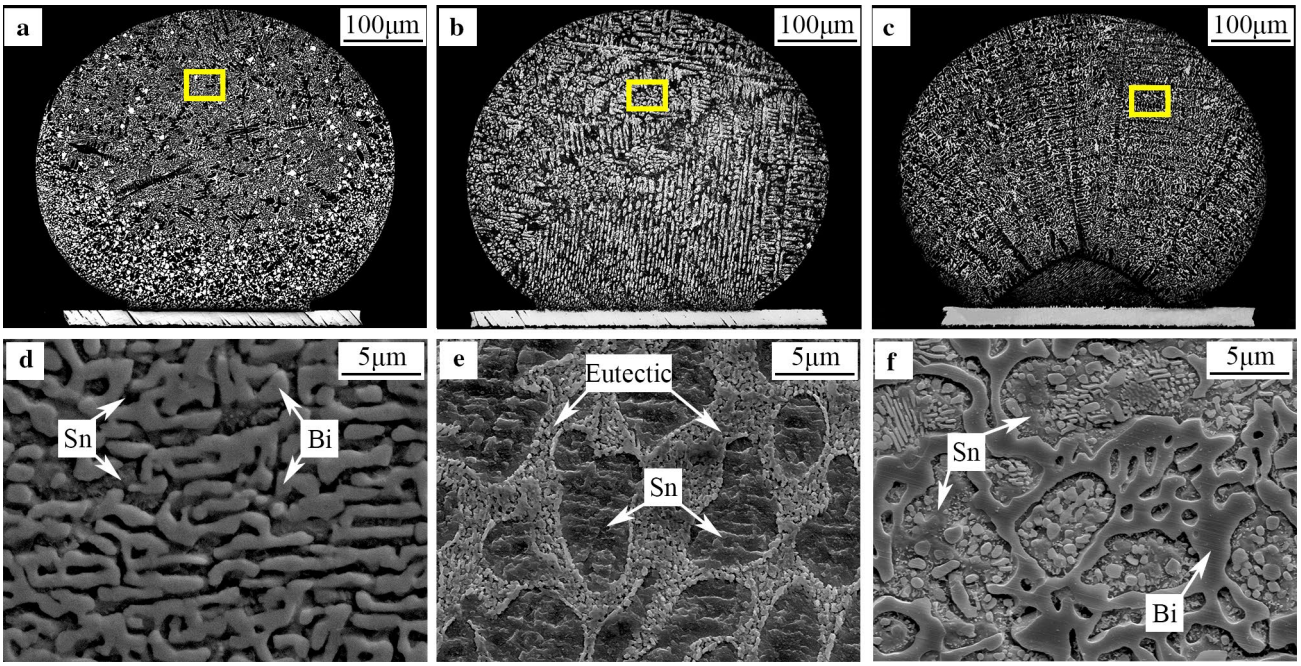

Fig. 2 Microstructure and EDS of as-soldered joints **a**–**c** optical morphology of the SnBi/Cu, SAC/Cu and SnBi/SAC/Cu joint, **d**–**f** SEM morphology of the SnBi/Cu, SAC/Cu and SnBi/SAC/Cu solder bulk

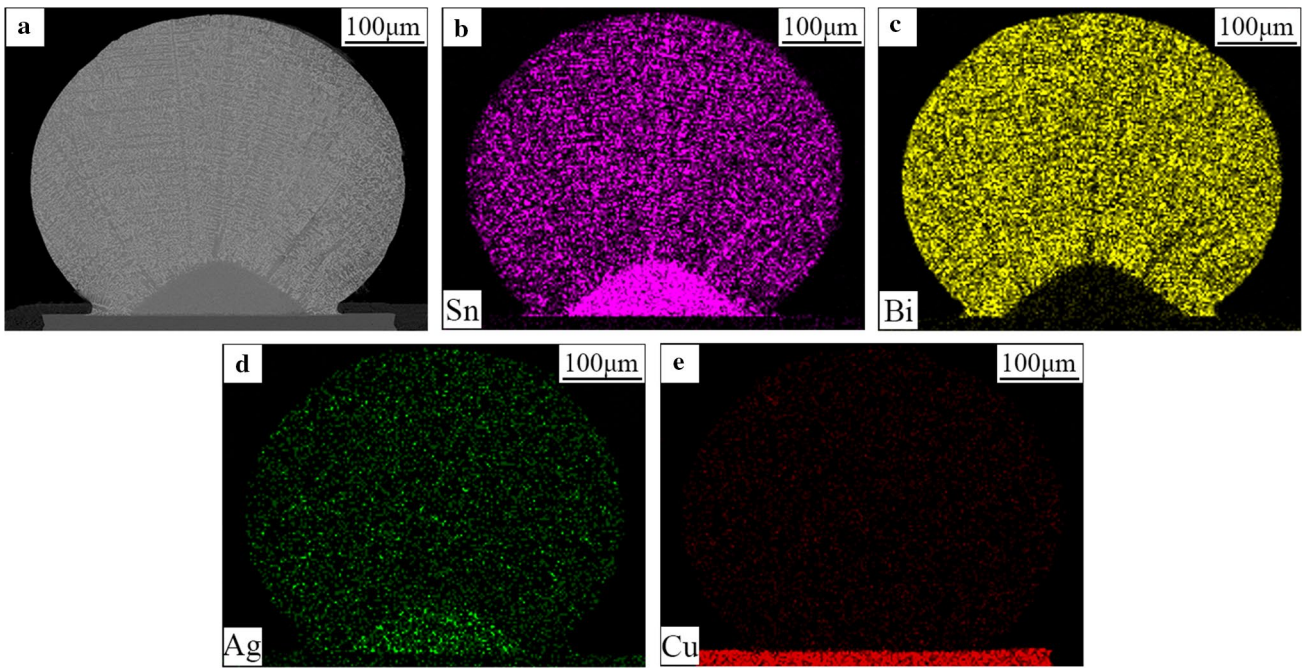

Fig. 3 SEM morphology and elemental mapping of the as-reflowed SnBi/SAC/Cu joint **a** microstructure, **b** element mapping of Sn, **c** element mapping of Bi, **d** element mapping of Ag, **e** element mapping of Cu

Ag atoms can be more strongly detected in the SAC solder bulk as shown in Fig. 3b, d. In contrast, Fig. 3c illustrates that Bi atom is mainly located in the SnBi bulk. Since the concentration of Cu in the Cu pad is much higher than that in the solder bulk, the element mapping of Cu is not very clear in Fig. 3e. As previously introduced, SAC alloy was

firstly soldered onto the Cu pad at 260 °C. Then the SnBi solder bulk was obtained on the SAC bulk at the soldering temperature of 160 °C. According to the research by Tan et al. [15], the melting temperature of SAC alloy ranges from 217 to 220 °C. Hence, the SAC bulk would not melt during this subsequent soldering process since its melting point is much higher than 160 °C. Therefore, the solid–liquid diffusion between SAC and SnBi is considered as the dominant inter-reaction mechanism.

Figure 4 shows the element mapping at the SnBi/SAC interface. As demonstrated in the figure, Sn, Ag, and Cu atoms diffuse from the SAC bulk into the molten SnBi during the soldering process. According to Fig. 4d, f, some of the Ag atoms react with Sn and form intermetallic compounds. Besides, minor Bi atoms could be detected in the SAC bulk, as shown in Fig. 4c. Kao [16] investigated the solid–liquid reaction between Cu and liquid Sn (and liquid Sn saturated with Cu). The reaction was under the control of both diffusion and dissolution. This finding could explain the results in Fig. 4. Firstly, Sn, Ag, and Cu atoms dissolve into the molten alloy as the liquid SnBi attaches to the solid SAC bulk in the soldering process. Therefore, the concentration of Sn, Ag, and Cu in the molten SnBi alloy increases. Secondly, diffusion becomes the dominant mechanism of the solid–liquid reaction between the SAC bulk and the molten SnBi saturated with dissolved Sn, Ag, and Cu atoms. As reported by Belyakov et al. [17], Bi atoms have high solubility of 20.5 wt% in β-Sn. It promotes the diffusion of Bi atoms into the SAC bulk as shown in Fig. 4c.

Figure 4b shows another interesting phenomenon. The element mapping of Sn presents continuous distribution at the SnBi/SAC interface, which means that the formation and growth of the β-Sn phases in SnBi is affected by the microstructure of β-Sn in the SAC bulk. It is approved by the microstructural observation in Fig. 2c. The β-Sn dendritic in SnBi grows along the SAC bulk like sunlight. This phenomenon is considered as a reason for the formation of large β-Sn grains in Fig. 2f. Meanwhile, the dissolution of Sn from SAC into SnBi increases the concentration of Sn in the molten SnBi alloy. As indicated by our previous studies [18, 19], the cooling curve of molten SnBi moves towards the Sn-rich side with the increased Sn concentration. This transformation facilitates the growth of the β-Sn phases in SnBi. It is suggested as another factor leading to the formation of the large β-Sn as shown in Fig. 2c.

Figure 5 shows the interfacial microstructure of the three kinds of solder joints. It is widely known that Cu_6Sn_5 is the main interfacial IMC in SnBi/Cu and SAC/Cu couples. As shown in Fig. 5a, Bi-rich phases densely distribute in the solder bulk of SnBi. The Bi-rich grains located on the interfacial IMC layer suppress the growth of Cu_6Sn_5. Therefore, the Cu_6Sn_5 IMC layer in SnBi/Cu is much thinner than that in the other two kinds of solder joints. The EDS results in Fig. 5d approve that the interfacial IMC in the SnBi/SAC/Cu solder joint is also Cu_6Sn_5. Compared with SAC/Cu, the composite solder joint shows larger interfacial IMC grains. As introduced in the experimental part, the SAC bulk in the composite solder joint was soldered with the same soldering

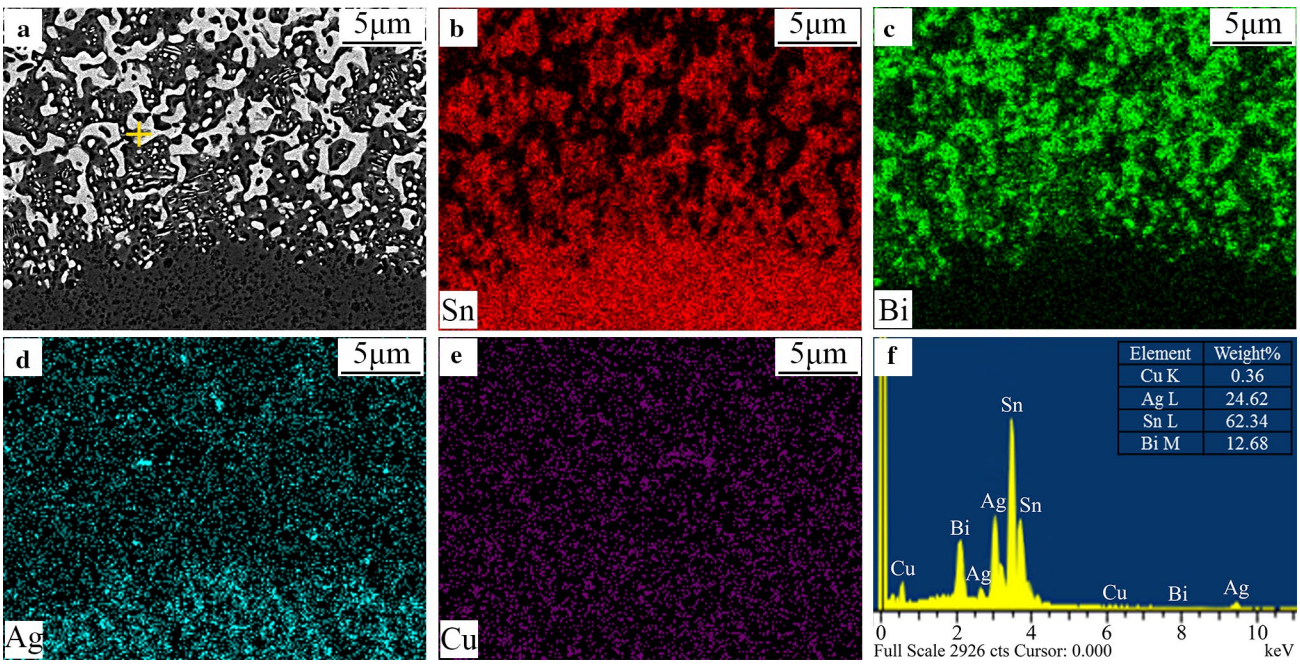

Fig. 4 Element mapping of the SnBi/SAC interface **a** microstructure, **b** element mapping of Sn, **c** element mapping of Bi, **d** element mapping of Ag, **e** element mapping of Cu, **f** EDS of the point

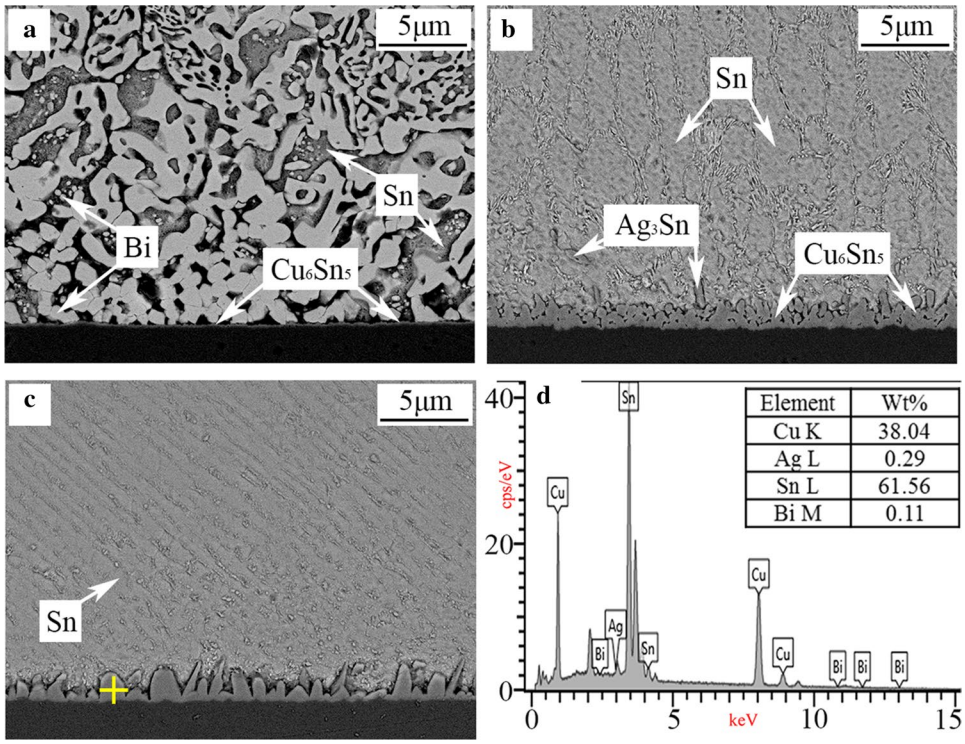

Fig. 5 Interfacial microstructure and EDS analysis of the solder joints **a** SnBi/Cu, **b** SAC/Cu, **c** SnBi/SAC/Cu, and **d** EDS of the point

parameters as the SAC/Cu solder joint. Then the SnBi alloy was soldered onto the SAC bulk to obtain the solder joint with superposition structure. This process promotes the ripening of the Cu_6Sn_5 interfacial IMC grains.

3.2 Shear behavior of the solder joints

Figure 6a shows the average shear force of the solder joints. Here the shear height was 45 μm and the shear speed was 0.1 mm/s. As shown in the figure, the average shear force of the SnBi/Cu solder joints is near 14 N. Compared with this, the SnBi/SnAgCu/Cu solder joints with superposition structure show slightly lower shear force. Among all the three types of solder joint, the shear force of SAC/Cu is the lowest. Figure 6b presents the typical force-distance relationships of the solder joints during the shear test. The shear force of SnBi/Cu presents a sharp decrease after the peak point, which implies the occurrence of brittle fracture in the SnBi solder joint. According to the microstructural observation in Fig. 2, plastic deformation of the solder material is suppressed due to the hard and brittle Bi-rich matrix. In contrast, the shear curve of SAC/Cu presents obvious plastic deformation of the solder material. As indicated by Di Maio and Hunt [20], β-Sn is ductile phase. Therefore, SAC/

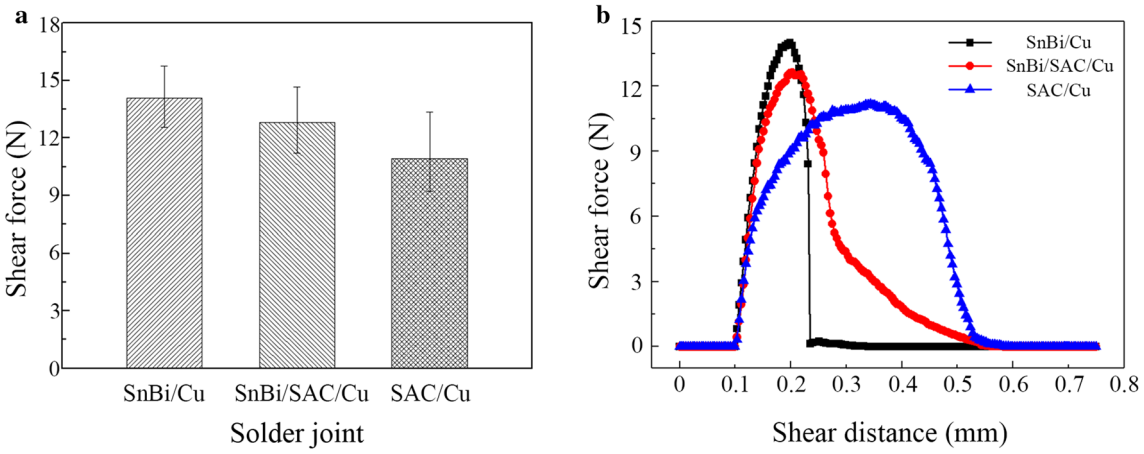

Fig. 6 Results of the shear test **a** shear force of three kinds of solder joints. **b** shear curves of three kinds of solder joints

Cu shows better ductility than SnBi/Cu due to its high concentration of β-Sn. As shown in Fig. 2, the concentration of β-Sn phase in the composite solder joints is much higher than that in the solder bulk of SnBi/Cu. Consequently, the composite solder joints show more ductile features than the SnBi/Cu solder joint does, as shown in Fig. 6b.

Figure 7 shows the fracture morphology of three kinds of solder joints. According to the magnified morphology presented in Fig. 7d, e, brittle fracture and ductile fracture is suggested to be the dominant failure mode of the SnBi/Cu and the SAC/Cu solder joints, respectively. The fracture morphology of the SnBi/SAC/Cu joint shows a composite failure mode including both brittle fracture and ductile fracture, as shown in Fig. 7f.

The shear fractures were observed by super resolution digital microscope. As presented in Fig. 8, all fractures occur near the interface of the solder joints. This phenomenon is reasonable since the soldering interface is considered as the weakest part in a solder joint. However, the height distribution images indicate that the highest height of the three fractures is different. Among the three solder joints, SnBi/Cu shows the lowest fracture height. As shown in Fig. 5, SnBi/Cu has the thinnest IMC layer due to the suppression of the Bi-rich matrix. Based on the discussion above, limited deformation appeared in the solder joint during the shear test. Therefore, brittle failure occurred near the soldering interface. Compared with SnBi/Cu, SAC/Cu shows much better ductility. The solder bulk deformed along the shear

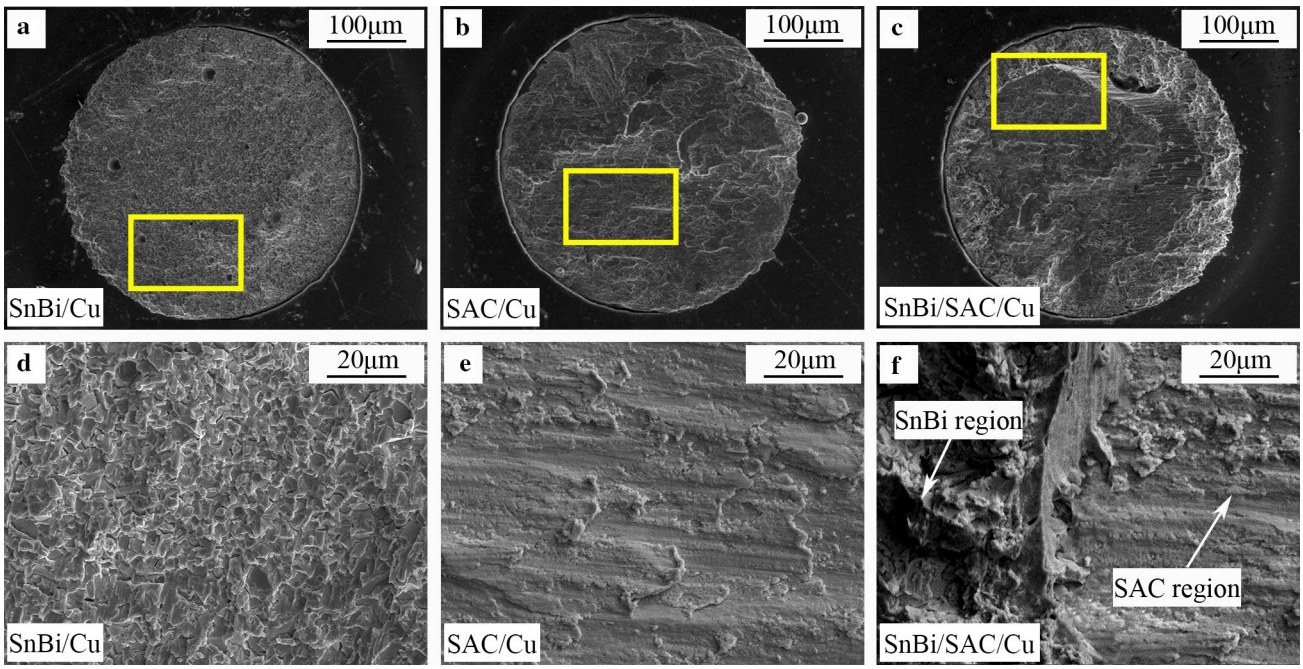

Fig. 7 The morphology of the shear fracture of three kinds of solder joints. **a** SnBi/Cu, **b** SAC/Cu, **c** SnBi/SAC/Cu, **d** magnified area in (**a**), (**e**) magnified area in (**b**), (**f**) magnified area in (**c**)

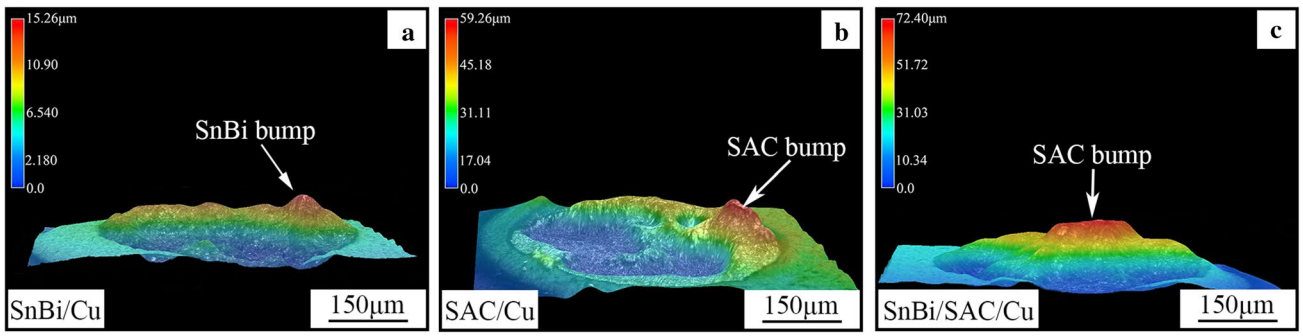

Fig. 8 Fracture morphology obtained by the super resolution digital microscope. **a** SnBi/Cu, **b** SAC/Cu, **c** SnBi/SAC/Cu

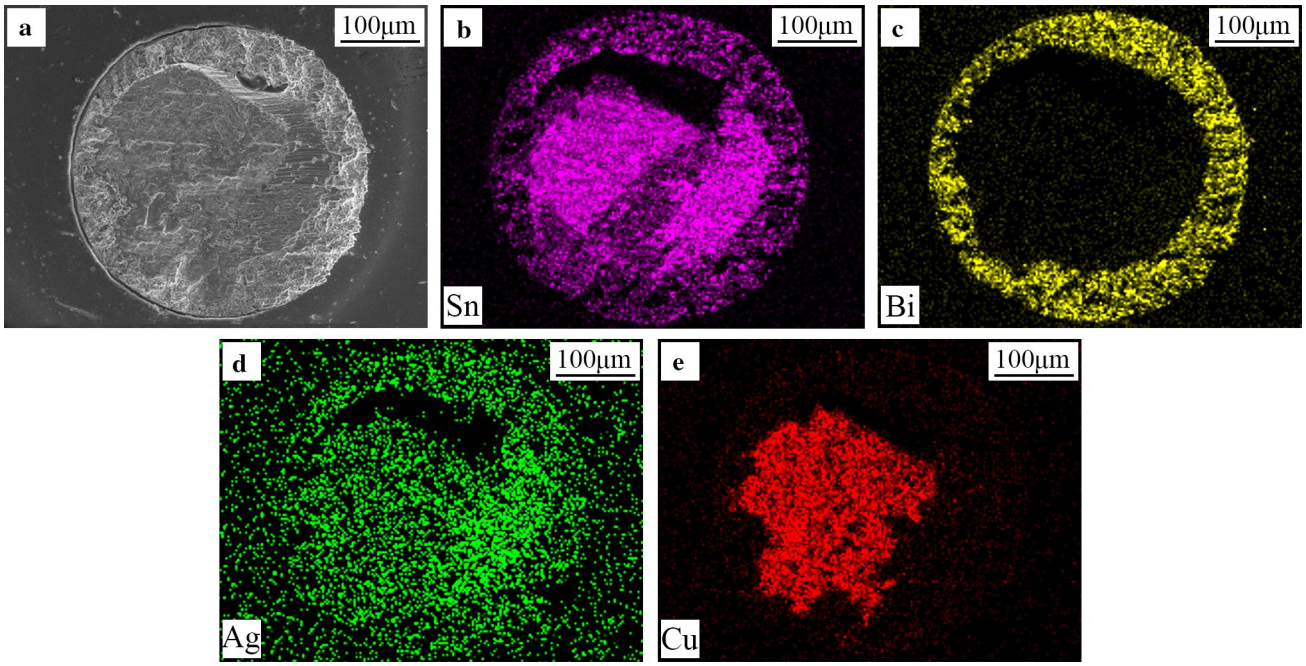

Fig. 9 SEM and element mapping of the shear fracture in SnBi/SAC/Cu joint. **a** Microstructure, **b** element mapping of Sn, **c** element mapping of Bi, **d** element mapping of Ag, **e** element mapping of Cu

direction during the shear test. Then the highest fracture height appears at the shear end of the solder joint as presented in Fig. 8b. As shown in Fig. 8c, the composite solder joint has higher fracture height than the other two kinds of solder joints. The highest height is located at the central area of the shear fracture.

Since the composite solder joint shows different shear morphology from the others, element mapping analysis was used to investigate its shear behavior, as shown in Fig. 9. It is clear that the central area of the fracture mainly consists of Sn, Ag, and Cu elements, indicating that the residue bump in Fig. 8c is formed by the SAC solder bulk. The surrounding area of this bump is composed of Sn, Bi, Ag, and Cu. Combined with the microstructure and shear analysis, this area is suggested to be the shear fracture in SnBi. Based on the discussion above, Ag and Cu dissolve from solid SAC bulk into molten SnBi during the soldering process. Thus Ag and Cu elements could be detected in this area. The fracture mechanism during the shear test could be described as follow: firstly, crack appeared at the SnBi/Cu interface as the shear force was loaded on the solder joint. Secondly, the cracks propagated through the SAC bulk as well as the SnBi/Cu interface around it. At last, the solder joint was totally sheared off when the crack extended to the end-side through the SnBi/Cu interface. According to the shear performance of the solder joints, it could be concluded that the SAC bulk in the composite solder joint effectively suppresses the brittle failure of SnBi eutectic solder joint.

4 Conclusions

The SAC bulk in the composite solder joint increased the concentration and grain size of β-Sn in the SnBi bulk. Tiny Bi-rich particles were observed in those β-Sn phases. Compared with the traditional SnBi solder joint, the brittle dense Bi-rich matrix was inhibited in the superposition structure. Failure analysis verified that the SnBi/SAC/Cu solder joint showed a composite failure mode including both brittle fracture and ductile fracture during the shear test. The SAC bulk worked as a barrier to the crack propagation. Consequently, the design of solder joint with superposition structure markedly suppresses the brittle interfacial failure of SnBi solder joint.

Acknowledgements This work is supported by National Natural Science Foundation of China (Grant No. 51604090) and Natural Science Foundation of Heilongjiang Province (Grant No. E2017050).

References

1. P.L. Liu, J.K. Shang, J. Mater. Res. **16**(6), 1651 (2001)
2. Y. Li, Y.C. Chan, J. Alloys Compd. **645**, 566 (2015)
3. D. Ma, P. Wu, Trans. Nonferr. Metal. Soc. **25**(4), 1225 (2015)
4. W. Zhu, Y. Ma, X. Li, W. Zhou, P. Wu, J. Mater. Sci.: Mater. Electron. **29**(9), 7575 (2018)
5. H. Sun, Y.C. Chan, F. Wu, J. Mater. Sci.: Mater. Electron. **26**(7), 5318 (2015)

6. Y. Liu, H. Fu, F. Sun, H. Zhang, X. Kong, T. Xin, J. Mater. Process. Technol. **238**, 290 (2016)
7. W.R. Myung, Y. Kim, S.B. Jung, J. Electron. Mater. **44**(11), 4637 (2015)
8. F. Wang, D. Li, Z. Zhang, M. Wu, C. Yan, J. Mater. Sci.: Mater. Electron. **8**(24), 19051 (2017)
9. F.Q. Hu, Q.K. Zhang, J.J. Jiang, Z.L. Song, Mater. Lett. **214**, 142 (2018)
10. H.F. Zou, Q.K. Zhang, Z.F. Zhang, Mater. Sci. Eng. A **532**, 167 (2012)
11. S. Zhou, Y.A. Shen, T. Uresti, V.C. Shunmugasamy, B. Mansoor, H. Nishikawa, J. Mater. Sci.: Mater. Electron. **30**(8), 7423 (2019)
12. L. Zhang, L. Sun, Y. Guo, J. Mater. Sci.: Mater. Electron. **26**(10), 7629 (2015)
13. T. Lu, D. Yi, H. Wang, X. Tu, B. Wang, J. Alloys Compd. **781**, 633 (2019)
14. G. Chen, L. Liu, J. Du, V.V. Silberschmidt, Y.C. Chan, C. Liu, F. Wu, J. Mater. Sci. **51**(22), 10077 (2016)
15. A.T. Tan, A.W. Tan, F. Yusof, J. Alloys Compd. **705**, 188 (2017)
16. C.R. Kao, Mater. Sci. Eng., A **238**(1), 196 (1997)
17. S.A. Belyakov, C.M. Gourlay, Thermochim. Acta **654**, 65 (2017)
18. Y. Liu, H. Fu, H. Zhang, F. Sun, X. Wang, G. Zhang, J. Mater. Sci.: Mater. Electron. **28**(24), 19113 (2017)
19. R. Xu, Y. Liu, H. Zhang, Z. Li, F. Sun, G. Zhang, J. Electron. Mater. **48**(3), 1758 (2019)
20. D. Di Maio, C. Hunt, J. Mater. Sci.: Mater. Electron. **20**(4), 386 (2008)